

# CONVERGENCE ANALYSIS OF THE INTRINSIC SURFACE FINITE ELEMENT METHOD

ELENA BACHINI AND MARIO PUTTI

**ABSTRACT.** The Intrinsic Surface Finite Element Method (ISFEM) was recently proposed to solve Partial Differential Equations (PDEs) on surfaces. ISFEM proceeds by writing the PDE with respect to a local coordinate system anchored to the surface and makes direct use of the resulting covariant basis. Starting from a shape-regular triangulation of the surface, existence of a local parametrization for each triangle is exploited to approximate relevant quantities on the local chart. Standard two-dimensional FEM techniques in combination with surface quadrature rules complete the ISFEM formulation thus achieving a method that is fully intrinsic to the surface and makes limited use of the surface embedding only for the definition of linear basis functions. However, theoretical properties have not yet been proved. In this work we complement the original derivation of ISFEM with its complete convergence theory and propose the analysis of the stability and error estimates by carefully tracking the role of the geometric quantities in the constants of the error inequalities. Numerical experiments are included to support the theoretical results.

Surface PDEs, Intrinsic Surface Finite Element Method, Convergence Theory  
[MSC 2010] 58J32, 65N30, 65N15

## 1. INTRODUCTION

Surface phenomena are ubiquitous in nature, playing an important role in mediating exchanges between contrasting media. They encompass a wide range of scales, from nano to planetary, with examples including earth processes [3, 7, 12–15], biological applications [20, 22, 24], and image processing [6, 27]. These models are typically based on partial differential equations (PDEs) governing balance laws of scalar, vector, and tensor quantities living on the surface. The detailed mathematical understanding of these PDEs is still limited, and applications are tackled by numerical techniques.

Most of the approaches developed so far for the discretization of surface PDEs rely heavily on the embedding in the ambient Euclidean space to project quantities back to the surface. In essence, the quantities of interest arising from the solution of the PDE are extended to a tubular neighborhood of the surface and then projected back to the surface or its piecewise approximation, thus avoiding altogether the need to use charts [23]. This strategy has allowed the development of conforming and nonconforming finite element methods using the so-called Surface Finite Element (SFEM) originally developed in [10] (see [11] for a recent review), with extensions to discontinuous Galerkin [2] and low order virtual element methods [16]. A different approach has been recently proposed in [4], where the Intrinsic Surface Finite Element Method (ISFEM) has been developed and favorably compared to the embedded approach of [11] for the surface advection-diffusion-reaction equation. A variant of this scheme has been used to develop arbitrary order virtual elements on surfaces [5], by working directly on the chart. This latter scheme works in a geometrically intrinsic setting but needs a complete knowledge of the parametrization.

The ISFEM method is based on piecewise linear approximations of the discrete spaces and relies exclusively on geometric quantities that are intrinsic to the surface by using information related only to the surface mesh and its piecewise affine approximation. The main advantage of ISFEM

with respect to the embedded approach is that the numerical solution, whether scalar or vector or tensor, is an object intrinsically defined on the surface, avoiding the need to define its extension in  $\mathbb{R}^3$  and its projection back to the surface. In addition, the formulation of the method does not require in principle the explicit knowledge of the parametrization but can be defined directly from a surface triangulation. Indeed, the ISFEM formulation in the scalar case requires only the knowledge of the tangent plane at the vertices of the surface triangulation in a form that can be exact, by means of the knowledge of the parametrization, or approximate, i.e., starting from point data. The embedding of the surface  $\Gamma$  in  $\mathbb{R}^3$  is used exclusively in the definition of the basis functions. These are calculated by projecting onto local tangent planes a first order polynomial defined either in the ambient space or on a local chart. All the other ingredients of the ISFEM scheme use intrinsic geometric quantities supposed to be known at the vertices of the surface triangulation. As a consequence, the method can freely use different embeddings (metrics), can be adapted to multiple charts if available, and, unlike SFEM or other approaches (see e.g. [23]), can be extended with few and straight-forward modifications to vector and tensor-valued PDEs.

In this paper we develop the full numerical analysis of ISFEM, not yet addressed in previous work. It turns out that, after verification of the density of the discrete ISFEM subspaces, the convergence estimates arise directly from the redefinition of an appropriate scalar product intrinsic to  $\Gamma$ . We start with the identification of a proper Local Coordinate System (LCS) anchored on the surface  $\Gamma$ , we discuss the weak formulation of the PDE written in covariant form and defined on appropriate surface Sobolev spaces, e.g.,  $H^1(\Gamma)$  for a closed surface without boundary or  $H_0^1(\Gamma)$  for a surface with homogeneous Dirichlet boundary. This operation introduces anisotropy due to the presence of the metric tensor arising from the first fundamental form of  $\Gamma$ . This anisotropy, whose ratio remains always bounded for a regular surface, adds to the eventual anisotropy of a tensor-valued diffusion coefficient. This added difficulty is counterbalanced by the fact that the ensuing numerical discretization, being defined on the LCS and thus on the chart or atlas, can exploit all the techniques developed for a planar two-dimensional domain and inherits all the related properties. For this reason, in our convergence estimates we discuss how the inequality constants depend upon the surface geometric quantities, intrinsic or extrinsic, i.e., depending on the first or second fundamental form. Our calculations show that optimal second order convergence is obtained under standard assumptions on the regularity of the mesh. This is experimentally discussed in the numerical results section, where convergence rates with respect to a manufactured solution are exposed and the behavior of the error constants at varying curvatures discussed. An example on a sphere defined by multiple charts is also presented.

## 2. THE INTRINSIC SURFACE FEM

Consider a compact surface  $\Gamma \subset \mathbb{R}^3$  over which we would like to solve an elliptic equation of the form:

$$(1) \quad -\nabla_{\mathcal{G}} \cdot (\mathbb{D} \nabla_{\mathcal{G}} u) = f \quad \text{on } \Gamma,$$

where  $\Gamma$  is assumed to be fixed in time and the solution  $u : \Gamma \rightarrow \mathbb{R}$  is a scalar function defined on the surface. The tensor  $\mathbb{D}$  is a rank-2 symmetric and positive-definite diffusion tensor, and we assume  $f \in L^2(\Gamma)$ . The differential operators  $\nabla_{\mathcal{G}} \cdot$  and  $\nabla_{\mathcal{G}}$ , the surface divergence and gradient, respectively, need to be properly defined to follow the geometric setting of the problem. If the compact surface has no boundary, eq. (1) is augmented by the constraints of zero mean on  $u$  and  $f$ . If the surface has boundary (i.e.,  $\partial\Gamma \neq \{\emptyset\}$ ) we assume zero Neumann conditions, again implicitly augmented by the zero mean constraints, or zero Dirichlet boundary conditions. For the handling of non-homogeneous boundary conditions we refer to [8].

**2.1. Geometrical setting.** Let  $\Gamma \subset \mathbb{R}^3$  be a 2-dimensional  $C^k$  regular surface. We recall that a surface  $\Gamma \subset \mathbb{R}^3$  is said to be  $C^k$  regular if for any point  $\mathbf{p} \in \Gamma$  there exists a map  $\phi_{\mathbf{p}} : U \rightarrow \mathbb{R}^3$

of class  $C^k$ , with  $U \subset \mathbb{R}^2$ , such that  $\phi_{\mathbf{p}}(U) \subset \Gamma$  is a neighborhood of  $\mathbf{p}$ , i.e., there exists an open neighborhood  $V \subset \mathbb{R}^3$  of  $\mathbf{p}$  for which  $\phi_{\mathbf{p}}(U) = V \cap \Gamma$ , and such that  $\phi_{\mathbf{p}}$  is a diffeomorphism of its image. The map  $\phi_{\mathbf{p}}$  is called a local parametrization centered in  $\mathbf{p}$ . The inverse of the parametrization,  $\phi_{\mathbf{p}}^{-1} : V \cap \Gamma \rightarrow U$ , is called a local chart in  $\mathbf{p}$ . Explicitly, we have the following transformations:

$$\begin{aligned} \phi : U &\longrightarrow V \cap \Gamma & \psi := \phi^{-1} : V \cap \Gamma &\longrightarrow U \\ \mathbf{s} &\longmapsto \mathbf{x} & \mathbf{x} &\longmapsto \mathbf{s} \end{aligned}$$

where  $\mathbf{s} = (s^1, s^2)$  are the local coordinates,  $\phi_{\mathbf{p}}(U)$  is the coordinate neighborhood, and  $\mathbf{x} = (x^1, x^2, x^3)$  are the global Cartesian coordinates of a point on the surface. Given two points  $\mathbf{p}, \mathbf{q} \in \Gamma$  and their local parametrizations  $\phi_{\mathbf{p}}, \phi_{\mathbf{q}}$ , with  $U_{\mathbf{p}} \cap U_{\mathbf{q}} \neq \emptyset$ , we say that the local parametrizations are compatible if the transition map  $\phi_{\mathbf{p}} \circ \phi_{\mathbf{q}}^{-1}$  is a  $C^k$  diffeomorphism. We assume to have a family  $\mathcal{A} = \{\phi_{\alpha}\}$  of compatible local parameterizations  $\phi_{\alpha} : U_{\alpha} \rightarrow \Gamma$  such that  $\Gamma = \cup_{\alpha} \phi_{\alpha}(U_{\alpha})$  (an atlas for  $\Gamma$ ).

Given a point  $\mathbf{p} \in \Gamma$ , the practical construction of the relevant objects proceeds as follows [3, 4]. We calculate the two tangent vectors  $\mathbf{t}_1(\mathbf{p})$  and  $\mathbf{t}_2(\mathbf{p})$  on  $T_{\mathbf{p}}\Gamma$ :

$$\hat{\mathbf{t}}_i(\mathbf{p}) = d\phi_{\mathbf{p}}(\mathbf{e}_j(\mathbf{p})) = \left( \frac{\partial x^1}{\partial s^i}, \frac{\partial x^2}{\partial s^i}, \frac{\partial x^3}{\partial s^i} \right), \quad i = 1, 2 \text{ and } j = 1, 2, 3,$$

where  $d\phi_{\mathbf{p}}$  is the Jacobian matrix of the coordinate transformation and  $\mathbf{e}_1(\mathbf{p}), \mathbf{e}_2(\mathbf{p}), \mathbf{e}_3(\mathbf{p})$  are the canonical basis vectors of  $\mathbb{R}^3$ . For numerical stability, the vector  $\hat{\mathbf{t}}_2$  is orthogonalized with respect to  $\hat{\mathbf{t}}_1$  via Gram-Schmidt, yielding the orthogonal frame  $\mathbf{t}_1, \mathbf{t}_2$  on  $T_{\mathbf{p}}\Gamma$ . The metric tensor is the diagonal matrix given by:

$$(2) \quad \mathcal{G}(\mathbf{p}) := \begin{pmatrix} \|\mathbf{t}_1(\mathbf{p})\|^2 & 0 \\ 0 & \|\mathbf{t}_2(\mathbf{p})\|^2 \end{pmatrix} = \begin{pmatrix} g_{11}(\mathbf{p}) & 0 \\ 0 & g_{22}(\mathbf{p}) \end{pmatrix}.$$

The metric defines the surface scalar product  $\langle \mathbf{u}, \mathbf{v} \rangle_{\mathcal{G}} = g_{ij}u^i v^j$ , and has inverse denoted by  $\mathcal{G}^{-1} = \{g^{ij}\}$ . It is possible to show [9] that there exist constants  $\mu_{*,\Gamma}$  and  $\mu_{\Gamma}^*$  such that:

$$\mu_{*,\Gamma} \|\mathbf{w}\|^2 \leq \langle \mathbf{w}, \mathbf{w} \rangle_{\mathcal{G}} \leq \mu_{\Gamma}^* \|\mathbf{w}\|^2 \quad \text{for } \mathbf{w} \in T_{\mathbf{p}}\Gamma,$$

where  $\mu_{*,\Gamma} = \min\{g_{11}, g_{22}\} \geq 1$  and  $\mu_{\Gamma}^* = \max\{g_{11}, g_{22}\}$  are the minimum and maximum eigenvalues of  $\mathcal{G}$ . Moreover, we have the following global uniform bounds on the norms and determinant of  $\mathcal{G}(\Gamma)$ :

$$(3) \quad c_{*,\Gamma} = \inf_{\mathbf{p} \in \Gamma} \|\mathcal{G}^{-1}(\mathbf{p})\|^2, \quad c_{\Gamma}^* = \sup_{\mathbf{p} \in \Gamma} \|\mathcal{G}^{-1}(\mathbf{p})\|^2, \quad g_{*,\Gamma} \leq \sqrt{\det(\mathcal{G}(\Gamma))} \leq g_{\Gamma}^*.$$

where  $g_{*,\Gamma} = \min_{\mathbf{p} \in \Gamma} \sqrt{g_{11}(\mathbf{p})g_{22}(\mathbf{p})} \geq 1$  and  $g_{\Gamma}^* = \max_{\mathbf{p} \in \Gamma} \sqrt{g_{11}(\mathbf{p})g_{22}(\mathbf{p})}$ . We will be using the symbol  $|\Pi_{\Gamma}|$  to denote the supremum over  $\Gamma$  of the norm of the second fundamental form. This value can be related to the curvatures of  $\Gamma$ .

*Differential operators.* Within this setting it is possible to define the relevant intrinsic differential operators. For the intrinsic gradient of a scalar function  $f$  we have  $\nabla_{\mathcal{G}} f = \mathcal{G}^{-1} \nabla f$ , and we can write the intrinsic divergence of a (contravariant) vector  $\mathbf{q} = q^1 \mathbf{t}_1 + q^2 \mathbf{t}_2$  as  $\nabla_{\mathcal{G}} \cdot \mathbf{q} = \nabla \cdot (\sqrt{\det(\mathcal{G})} \mathbf{q}) / \sqrt{\det(\mathcal{G})}$ . Note that here the flux vector  $\mathbf{q} = -\mathbb{D} \nabla_{\mathcal{G}} f$  in eq. (1) is a vector tangent to  $\Gamma$  for a general (symmetric) diffusion tensor  $\mathbb{D}$ . Moreover, if  $\mathbb{D} = \epsilon \mathbb{I}$ , eq. (1) becomes the classical Laplace-Beltrami operator, i.e.  $\nabla_{\mathcal{G}} \cdot (\mathbb{D} \nabla_{\mathcal{G}} f) = \epsilon \Delta_{\mathcal{G}} f$ , where:

$$\Delta_{\mathcal{G}} f = \nabla_{\mathcal{G}} \cdot \nabla_{\mathcal{G}} f = \frac{1}{\sqrt{g_{11}g_{22}}} \left[ \frac{\partial}{\partial s^1} \left( \sqrt{\frac{g_{22}}{g_{11}}} \frac{\partial f}{\partial s^1} \right) + \frac{\partial}{\partial s^2} \left( \sqrt{\frac{g_{11}}{g_{22}}} \frac{\partial f}{\partial s^2} \right) \right].$$

The standard tools deriving from Stokes theorems hold with the intrinsic operators without any modification. We first recall the formal definition of the integral of a function over a surface, which does not depend on the parametrization [1]:

**Definition 2.1.1.** *Let  $f : \Gamma \rightarrow \mathbb{R}$  be a continuous function defined on a regular surface  $\Gamma$  with parametrization given by  $\phi : U \rightarrow \Gamma$ . The integral of  $f$  on  $\Gamma$  is:*

$$\int_{\Gamma} f = \int_{\phi^{-1}(\Gamma)} (\tilde{f} \circ \phi) \sqrt{\det(\mathcal{G})} \, ds .$$

Then, the following intrinsic Green's formula holds:

$$(4) \quad \int_{\Gamma} \langle \mathbb{D} \nabla_{\mathcal{G}} u, \nabla_{\mathcal{G}} v \rangle_{\mathcal{G}} = - \int_{\Gamma} \nabla_{\mathcal{G}} \cdot (\mathbb{D} \nabla_{\mathcal{G}} u) v + \int_{\partial\Gamma} \langle \mathbb{D} \nabla_{\mathcal{G}} u, \mu \rangle_{\mathcal{G}} v ,$$

where  $\mu : \Gamma \rightarrow \mathbb{R}^2$  denotes the vector tangent to  $\Gamma$  and normal to  $\partial\Gamma$  with components written with respect to the curvilinear reference frame (i.e.  $\mu = \mu^1 \mathbf{t}_1 + \mu^2 \mathbf{t}_2$ ).

**Remark 2.1.2.** *Throughout the paper, we identify  $\Gamma$  with its local chart making sure to distinguish when we work on  $V \cap \Gamma$  or on  $U$  by proper use the parametrization  $\phi_{\mathbf{p}}$  and its inverse. Note that our intent is to maintain as much as possible the definitions of all the operations of our scheme on the LCS defined on  $\Gamma$ . To this aim, surface functions  $f : \Gamma \rightarrow \mathbb{R}$  are written in the LCS and need to be integrated with respect to  $dV_{\mathcal{G}}$ , the volume form induced by the metric  $\mathcal{G}$ . As a consequence, our numerical scheme is defined directly on the surface and exploits the two-dimensional structure of the reference system carried by the parametrization. To achieve our goal of minimizing the use of the knowledge of the parametrization, we need to introduce surface quadrature rules defined directly on  $V \cap \Gamma$ . On the other hand, the numerical analysis of the scheme exploits the results already known for domains in  $\mathbb{R}^2$  and for this reason we find it easier and cleaner to work on  $U \subset \mathbb{R}^2$ , i.e., the domain of the parametrization  $\phi_{\mathbf{p}}$ . This is achieved by formally using the inverse parametrization and the relation  $dV_{\mathcal{G}} = \sqrt{\det(\mathcal{G})} \, ds$ , so that integrals can be expressed with respect to the standard two-dimensional Lebesgue measure  $ds$ , as provided in definition 2.1.1.*

**2.2. Intrinsic variational formulation.** Without loss of generality we assume that  $\Gamma$  is described by a single (global) parametrization  $\phi : U \rightarrow \Gamma$ . The ensuing results and the definitions extend directly to the case of a surface defined by an atlas assuming, as mentioned before, that the necessary transition maps are smooth.

*Function spaces.* We use standard definitions and notations for Sobolev spaces [9], which can be directly extended to a compact manifold  $\Gamma$  (see [18, 28]). We denote with  $L^2(\Gamma)$  and  $H^1(\Gamma)$  the classical Hilbert spaces on  $\Gamma$ . Explicitly:

$$L^2(\Gamma) = \left\{ v : \Gamma \rightarrow \mathbb{R} : \int_{\Gamma} v^2 < \infty \right\}, \quad H^1(\Gamma) = \left\{ v \in L^2(\Gamma) : \nabla_{\mathcal{G}} v \in (L^2(\Gamma))^2 \right\} .$$

Norms in  $L^2(\Gamma)$  and  $H^1(\Gamma)$  are denoted with  $\|\cdot\|_{L^2(\Gamma)}$  and  $\|\cdot\|_{H^1(\Gamma)}$ , respectively, and are given by:

$$\|v\|_{L^2(\Gamma)}^2 = \int_{\Gamma} v^2 \quad \text{and} \quad \|v\|_{H^1(\Gamma)}^2 = \int_{\Gamma} v^2 + \int_{\Gamma} |\nabla_{\mathcal{G}} v|_{\mathcal{G}}^2 ,$$

where  $|\nabla_{\mathcal{G}} v|_{\mathcal{G}}^2 = \langle \nabla_{\mathcal{G}} v, \nabla_{\mathcal{G}} v \rangle_{\mathcal{G}}$ . We will also use the  $H^2$ -seminorm given by:

$$|v|_{H^2(\Gamma)}^2 = \int_{\Gamma} |\nabla^2 v|_{\mathcal{G}}^2 ,$$

where  $|\nabla^2 v|_{\mathcal{G}} = \text{tr}((\mathcal{G}^{-1} \nabla^2 v)^2)$  with  $\nabla^2 v$  being the second covariant derivative of  $v$ . We note that:

$$\int_{\Gamma} |\nabla^2 v|_{\mathcal{G}}^2 \leq c_{\Gamma}^{*2} \left[ \int_{\Gamma} |\partial^2 v|^2 + C_{\phi}^2 |\mathbb{I}_{\Gamma}|^2 \int_{\Gamma} |\partial v|^2 \right] ,$$

where  $C_\phi$  is a generic constant depending on the parametrization, from which, recalling that  $(\Delta_\mathcal{G} v)^2 = [\text{tr}(\mathcal{G}^{-1} \nabla^2 v)]^2 \geq \text{tr}((\mathcal{G}^{-1} \nabla^2 v)^2)$ , it is easy to prove that the following holds:

$$(5) \quad c \|\partial^2 v\|_{L^2}^2 \leq |v|_{H^2}^2 \leq C \|\Delta_\mathcal{G} v\|_{L^2}^2 .$$

Note that the above inequalities are written without reference to the domain as they can be set equally on the surface  $\Gamma$  or the chart  $\phi^{-1}(\Gamma) = U$ .

*Intrinsic variational problem.* Now we can write the intrinsic variational formulation of the elliptic equation (1) in the LCS as:

**Problem 2.2.1.** Find  $u \in H^1(\Gamma)$ , with  $\bar{u} = 0$ , such that:

$$a(u, v) = F(v) \quad \forall v \in H^1(\Gamma) ,$$

where the “stiffness” bilinear form and the “forcing” linear form are given by:

$$a(u, v) = \int_\Gamma \langle \mathbb{D} \nabla_\mathcal{G} u, \nabla_\mathcal{G} v \rangle_\mathcal{G} \quad \text{and} \quad F(v) = \int_\Gamma f v .$$

Note that this is the direct extension to the surface  $\Gamma$  of the classical variational formulation of eq. (1). All the integrals are still written in intrinsic coordinates of our LCS.

*Poincaré inequality.* The dependence of the constants on the geometric characteristics of the surface originates mainly from the use of Poincaré inequality, which is given without proof in the following lemma.

**Lemma 2.2.2.** Let  $\Gamma$  a  $C^1$ -regular surface without boundary and let  $u \in H^1(\Gamma)$  be a function with average given by  $\bar{u} = \frac{1}{|\Gamma|} \int_\Gamma u$ . Then, there exists a constant  $C_\Gamma > 0$  such that:

$$\|u - \bar{u}\|_{L^2(\Gamma)} \leq C_\Gamma \|\nabla_\mathcal{G} u\|_{L^2(\Gamma)} \quad \forall u \in H^1(\Gamma)$$

Poincaré inequality can be adapted to surfaces with Neumann or Dirichlet boundaries in the usual way (see, e.g., [8]). From now on we assume for simplicity that  $\bar{u} = 0$ . As a consequence, the  $L^2$  the  $H^1$  norms are equivalent, as stated in the next straight-forward corollary.

**Corollary 2.2.3.** Let  $\Gamma$  a  $C^1$ -regular surface and let  $u \in H^1(\Gamma)$  be a function with zero average,  $\bar{u} = \frac{1}{|\Gamma|} \int_\Gamma u = 0$ . Then, the following inequalities hold:

$$\|\nabla_\mathcal{G} u\|_{L^2(\Gamma)} \leq \|u\|_{H^1(\Gamma)} \leq \sqrt{1 + C_\Gamma^2} \|\nabla_\mathcal{G} u\|_{L^2(\Gamma)} .$$

Next we want to give detailed expressions of the constant  $C_\Gamma$  as a function of the geometric characteristics of  $\Gamma$ . We recall that the best Poincaré constant is related to the first nonzero eigenvalue of the Laplace-Beltrami operator on  $\Gamma$ . Indeed, it is easy to see that  $C_\Gamma^2 = \lambda_1^{-1}$ . Thus, we need to distinguish the three cases of a compact surface with no boundary, a surface with Dirichlet boundary  $\partial\Gamma_D$  and a surface with Neumann boundary  $\partial\Gamma_N$ . Typically, bounds on these eigenvalues are given in terms of the Ricci curvature, but we note that for surfaces in  $\mathbb{R}^3$  the Ricci and the Gaussian curvature coincide up to a positive multiplicative constant. For this reason we state everything in terms of the latter. We can summarize these results in the following lemma, whose proof can be found in [19].

**Lemma 2.2.4.** Let  $\Gamma$  be a regular surface with Gaussian curvature  $\kappa$  bounded from below by a constant  $-R$  ( $R > 0$ ), and denote by  $\rho(\Gamma)$  the longest geodesic distance between two points. Then, there exist two positive constants  $C_1$  and  $C_2$  such that:

$$\lambda_1^N \geq \frac{C_1}{\rho(\Gamma)^2} \exp(-C_2 \rho(\Gamma) \sqrt{R}), \quad \text{and} \quad \lambda_1^D \geq \frac{C_1}{\rho(\Gamma)^2} \exp(-C_2(1 + \rho(\Gamma) \sqrt{R})),$$

where  $\lambda_1^N$  identifies the case of a compact surface without boundary or with Neumann boundary and  $\lambda_1^D$  the case of Dirichlet boundary.

In what follows we will characterize all the constants in the ensuing inequalities by explicitly keeping track of  $C_\Gamma$  to quantify the geometrical effects of the properties of the surface domain on the error estimates.

*Well-posedness.* We list here the classical assumptions on the continuity and coercivity of the bilinear form and continuity of the linear form defining the weak formulation 2.2.1. For  $a(\cdot, \cdot)$  we need the obvious hypothesis that the diffusion tensor  $\mathbb{D}$  be positive definite, i.e., there exist two positive constants  $d_*$  and  $d^*$  such that

$$(6) \quad d_* \|\mathbf{w}\|_{\mathcal{G}}^2 \leq \langle \mathbb{D}\mathbf{w}, \mathbf{w} \rangle_{\mathcal{G}} \leq d^* \|\mathbf{w}\|_{\mathcal{G}}^2 \quad \text{for all } \mathbf{w} \in T_{\mathbf{p}}\Gamma \quad \text{and for all } \mathbf{p} \in \Gamma.$$

Then we can state the following lemma.

**Lemma 2.2.5.** *The bilinear form  $a(\cdot, \cdot)$  in problem 2.2.1 is coercive and continuous, i.e., for any  $u, v \in H^1(\Gamma)$  the following inequalities hold:*

$$(7) \quad a(u, u) \geq \frac{d_*}{1 + C_\Gamma^2} \|u\|_{H^1(\Gamma)}^2, \quad |a(u, v)| \leq d^* \|u\|_{H^1(\Gamma)} \|v\|_{H^1(\Gamma)}.$$

Moreover, the linear form  $F(\cdot)$  is continuous:

$$F(v) \leq \|f\|_{L^2(\Gamma)} \|v\|_{L^2(\Gamma)}.$$

*Proof.* The proof is a standard application of the equivalence between the  $L^2$  and  $H^1$  norms in corollary 2.2.3 and the inequalities in eq. (7) :

$$a(u, u) = \int_{\Gamma} \langle \mathbb{D} \nabla_{\mathcal{G}} u, \nabla_{\mathcal{G}} u \rangle_{\mathcal{G}} \geq d_* \|\nabla_{\mathcal{G}} u\|_{L^2(\Gamma)}^2 \geq \frac{d_*}{1 + C_\Gamma^2} \|u\|_{H^1(\Gamma)}^2.$$

For the continuity we write:

$$|a(u, v)| \leq \|\mathbb{D} \nabla_{\mathcal{G}} u\|_{L^2(\Gamma)} \|\nabla_{\mathcal{G}} v\|_{L^2(\Gamma)} \leq d^* \|u\|_{H^1(\Gamma)} \|v\|_{H^1(\Gamma)}.$$

The continuity of  $F(\cdot)$  is simply an application of the Cauchy-Schwarz inequality.  $\square$

Under the above assumptions, the Lax-Milgram theorem holds:

**Lemma 2.2.6** (Lax-Milgram theorem). *Let  $\mathcal{V}(\Gamma)$  be a Hilbert space and  $a : \mathcal{V}(\Gamma) \times \mathcal{V}(\Gamma) \rightarrow \mathbb{R}$  be a continuous and coercive bilinear form. For all continuous linear forms  $F : \mathcal{V}(\Gamma) \rightarrow \mathbb{R}$  there exists a unique function  $u \in \mathcal{V}(\Gamma)$  such that:*

$$a(u, v) = F(v) \quad \forall v \in \mathcal{V}(\Gamma).$$

**2.3. Intrinsic finite element method.** Before going into the analysis of ISFEM, we would like to describe the principal steps that form the ISFEM approach. We recall that our guiding principle that justifies certain choices is to maintain the scheme as intrinsic as possible, i.e., we want to use only intrinsic geometric quantities and use the surface embedding and the parametrization as little as possible.

*The surface triangulation.* Let  $\mathcal{T}_h(\Gamma) = \cup_{i=1}^{N_T} T_i = \text{cl}(\Gamma)$  be a given geodesic surface triangulation of  $\Gamma$ , formed by the union of non-intersecting surface triangles. We denote by  $\Gamma_h$  or  $\mathcal{T}_h(\Gamma_h)$  the piecewise linear approximation of  $\Gamma$ , i.e., the union of 2-simplices in  $\mathbb{R}^3$  having the same vertices of  $\mathcal{T}_h(\Gamma)$  and characterized by the mesh parameter  $h$ , the length of the longest chord between two triangle vertices in  $\mathcal{T}_h(\Gamma)$ . We assume that  $\mathcal{T}_h(\Gamma_h)$  is shape-regular, i.e., there exists a constant  $c > 0$  independent of  $h$  such that  $r_T/h_T \geq c$  for all  $T_h \in \mathcal{T}_h(\Gamma_h)$ , where  $r_T$  is the radius of the circle inscribed in  $T_h$  and  $h_T$  is the longest side of  $T_h$ . By assumption,  $\mathcal{T}_h(\Gamma_h)$  is a closely inscribed triangulation in the sense of [21], or equivalently, in the sense of [11], which means that  $\mathcal{T}_h(\Gamma_h) \subset \mathcal{N}_\delta$ , where  $\mathcal{N}_\delta$  is a tubular neighborhood of  $\Gamma$  of radius  $\delta$  such that every point  $\mathbf{p} \in \mathcal{N}_\delta$

has a unique orthogonal projection onto  $\Gamma$ . As a consequence, for every flat cell  $T_h \subset \Gamma_h$  there corresponds a unique curved cell  $T \subset \Gamma$ , and this correspondence is bijective.

We will need to distinguish surface objects if described with respect to our LCS or with respect to the Cartesian coordinate system of  $\mathbb{R}^3$ . To this aim, a tilde above symbols of surface objects identifies their description with respect to the Cartesian coordinate system in  $\mathbb{R}^3$ . For example,  $\Gamma$ ,  $T$  and  $\tilde{\Gamma}$ ,  $\tilde{T}$  will be used to identify the same objects, the surface or a geodesic triangle, when expressed with respect to the LCS or the Cartesian coordinate system, respectively. Also, we will need the assumption that each cell  $T$  is contained in a single local parametrization. Recalling remark 2.1.2, we will denote with  $f$  a generic scalar function written with respect to the LCS, and with  $\tilde{f}$  and  $\check{f}$  the same function written with respect to  $U \subset \mathbb{R}^2$  and the standard Cartesian reference system of  $\mathbb{R}^3$ , respectively.

*Intrinsic spatial discretization.* Formally, we would like to work with the finite-dimensional  $\mathcal{P}_1$ -conforming FEM space  $\mathcal{V}_h(\mathcal{T}_h(\Gamma)) \subset H^1(\Gamma)$  given by:

$$(8) \quad \mathcal{V}_h(\mathcal{T}_h(\Gamma)) = \{v_h \in C^0(\mathcal{T}_h(\Gamma)) \text{ such that } v_h|_T \in \mathcal{P}_1(T) \quad \forall T \in \mathcal{T}_h(\Gamma)\}.$$

However, this definition is meaningless since we do not know how to define  $\mathcal{P}_1(T)$ , namely the space of first order polynomials in  $T$  with which we want to interpolate our solution. One way to circumvent this problem is proposed in [25, 26], where surface barycentric coordinates are used to generalize the classical linear interpolation on the surface. In this case the basis functions are nonlinear and their calculation requires the solution of local cell-wise quadratic minimization problems. Another approach is used in [5], where the equations, the variational formulation, and the VEM bilinear forms are defined on the chart. In case, two-dimensional Lagrangian linear basis functions can be defined in the usual way directly on the chart and can be used to evaluate the needed integrals. This approach requires complete knowledge of the surface parametrization, since a triangulation of the chart is needed. On the other hand, the ISFEM scheme in [4] does not use of the knowledge of the parametrization but only of the tangent planes at triangle vertices. Maintaining the goal of ISFEM to make use of the surface embedding and parametrization as little as possible, the following strategy for the definition of the basis functions can be devised. We work on an element-by-element basis as typical of FE methods and require the nodal ISFEM functions restricted on the surface triangle  $T$  to satisfy the classical interpolation property:

$$(9) \quad \varphi_j^T(\mathbf{p}_i) = \delta_{ij} \quad i, j = 1, 2, 3,$$

where  $\mathbf{p}_i \in \Gamma$  are the nodes of  $T$ . Given the global coordinates  $\mathbf{x}(\mathbf{p})$  of  $\mathbf{p} \in T$ , we define the affine function

$$(10) \quad \tilde{\varphi}_j^T(\mathbf{x}) = \tilde{a} + \tilde{b}x^1 + \tilde{c}x^2 + \tilde{d}x^3$$

as a function in  $\mathbb{R}^3$ . The coefficients can be calculated by imposing the fulfillment of eq. (9) plus the condition of passing through the point  $\mathbf{q} = \mathbf{p}_j + \mathbf{N}(\mathbf{p}_j)$  at unit distance from  $\mathbf{p}_j$  in the direction normal to the surface at  $\mathbf{p}_j$ . Given a surface triangle  $T \subset \Gamma$ , the regularity of  $\Gamma$  ensures the existence of a local chart  $U \subset \mathbb{R}^2$  with parametrization  $\phi_h$ , where we can find a triangle  $U_h \subset U$  such that  $\phi_h : U_h \rightarrow T$  with  $U_h \cong T_h$ . This allows us to define the nonlinear basis function  $\varphi_j^T := \tilde{\varphi}_j^T \circ \phi_h : U_h \rightarrow \mathbb{R}$  on this chart. Recall that we need to know the values of the basis functions and its derivatives only at the quadrature points  $\mathbf{r}_i$ , e.g. the triangle vertices if using the trapezoidal rule. These are readily known without the need to use the parametrization. Indeed, for the function values we use the interpolation property of the nonlinear functions  $\varphi_j^T$ . Instead, for the gradients, to maintain optimal accuracy we can consider only the linear part of  $\varphi_j^T$  obtained by projection onto the tangent planes defined at the quadrature points. Since  $\phi_{h,\mathbf{r}_i}(U_h) = T_{\mathbf{r}_i}\Gamma + \mathcal{O}(h^2)$  optimal convergence is retained.

**Remark 2.3.1.** *The definition of the basis function  $\tilde{\varphi}_j^T$  is the only phase of ISFEM in which the embedding of  $\Gamma$  in  $\mathbb{R}^3$  is explicitly used. All the other phases require only the knowledge of the tangent vectors spanning the tangent planes at the triangle vertices, thus requiring only intrinsic geometric quantities. Notice that, if the above projection of the nonlinear basis function  $\varphi_j^T$  is done on the plane containing  $T_h$ , the Surface FEM approach described in [11] is obtained.*

Now, it is easy to see that the set  $\{\varphi_j^T\}_{j=1}^3$  spans  $\mathcal{V}_h(T_h)$ , which can be used as ISFEM basis for  $\mathcal{V}_h(T)$  as the following density lemma shows.

**Lemma 2.3.2.** *Let  $\{\bar{\varphi}_j^T\}_{j=1}^3$  be the  $\mathcal{P}_1$  Lagrangian basis functions of  $\mathcal{V}_h(T)$  defined in  $U_h = \phi_h^{-1}(T)$ , then:*

$$\|\varphi_j^T - \bar{\varphi}_j^T\|_{L^2(U_h)} \leq C_\phi |\Pi_T| h_T^2,$$

where  $C_\phi$  is a generic constant depending on the parametrization.

*Proof.* On the local chart  $U_h$  we can build a set of classical  $\mathcal{P}_1$  Lagrangian basis functions  $\{\bar{\varphi}_j^T\}_{j=1}^3$ , which span all the affine functions on  $T_h$ . We can expand the parametrization locally at  $\mathbf{r}$  as:

$$\phi_{h,\mathbf{r}}(\mathbf{s}) = \mathbf{x}(\mathbf{r}) + \nabla \phi_{h,\mathbf{r}}(\mathbf{r}) \cdot \mathbf{x} + \frac{1}{2} \mathbf{x}^T \mathbf{H}_{\phi_h}(\mathbf{r}) \mathbf{x} + \mathcal{O}(h_T^3),$$

where  $\mathbf{H}_{\phi_h}$  is the Hessian of the parametrization, and  $\mathbf{x} = \phi_h(\mathbf{s})$ . The composition of  $\tilde{\varphi}_j^T$  defined in eq. (10) with the linear part on the right-hand-side of the above equation gives a linear function from  $U_h$  to  $\mathbb{R}$  that satisfies the interpolation property and thus coincides with  $\bar{\varphi}_j^T$ . The result thus follows by noting that the second order remainder can be bounded by:

$$\left\| \frac{1}{2} \mathbf{x}^T \mathbf{H}_{\phi_h}(\mathbf{r}) \mathbf{x} \right\| \leq C_\phi |\Pi_T| h_T^2.$$

□

**Remark 2.3.3.** *The last lemma implies that any function that satisfies the interpolation property and reproduces exactly linear functions when projected on the local tangent plane can be used as ISFEM  $\mathcal{P}_1$ -basis function. Hence, the construction described above is only one of the many possible examples. We will see another possibility in the numerical section when dealing with the stereographic projection on the sphere.*

The last step in the definition of our global basis functions  $\varphi_k$ ,  $k = 1, \dots, N^{dof}$ , is to glue together as usual the elemental components. Note that, because of the interpolation property, the resulting global basis functions are obviously conforming, albeit known only at the vertices. In conclusion, every function  $v_h$  in the functional space  $\mathcal{V}_h(\mathcal{T}_h(\Gamma))$  can be written as:

$$(11) \quad v_h(\mathbf{s}) = I_h(v_h)(\mathbf{s}) = \sum_{k=1}^{N^{dof}} v_k \varphi_k(\mathbf{s}) \quad \mathbf{s} \in \Gamma,$$

where  $I_h(v_h)$  indicates the ISFEM interpolant of  $v_h$ , and  $v_k$  are the nodal coefficients. Hence, the intrinsic FEM variational formulation can be written in the LCS as:

**Problem 2.3.4.** *Find  $u_h \in \mathcal{V}_h(\mathcal{T}_h(\Gamma))$  such that*

$$a(u_h, v_h) = F(v_h) \quad \forall v_h \in \mathcal{V}_h(\mathcal{T}_h(\Gamma)),$$

where the linear and bilinear forms are given by:

$$a(u_h, v_h) = \int_{\Gamma} \langle \mathbb{D} \nabla_{\mathcal{G}} u_h, \nabla_{\mathcal{G}} v_h \rangle_{\mathcal{G}} \quad \text{and} \quad F(v_h) = \int_{\Gamma} f_h v_h.$$



*Surface quadrature rules.* Up to the definition of the test space  $\mathcal{V}_h(\mathcal{T}_h(\Gamma))$ , no numerical approximations are done until this point, since all the operators and integrals are defined on  $\mathcal{T}_h(\Gamma)$  whose interior coincides with the surface  $\Gamma$ . We would like to remain within this setting as much as possible. Approximation issues arise when we need to practically compute quantities. To this aim, we assume that all the relevant geometric information related to the surface are known in exact or approximate (but consistent) form at the vertices of the triangulation and proceed by defining appropriate quadrature rules. In order to maintain optimal second order accuracy we need to provide quadrature rules whose error is locally proportional to  $h_T^2$ . Thus we can consider surface extensions of the trapezoidal and the mid-point quadrature rules for triangles, as developed in [17], as modified and effectively used in [3, 4]. In this work we consider the trapezoidal rule given by:

$$(12) \quad \int_T f \approx Q_h(f) = \frac{1}{3} \sum_{j=1}^3 f(\mathbf{p}_j) \mathcal{A}_{T_h},$$

where  $\mathcal{A}_{T_h}$  is the cell area and  $f(\mathbf{p}_j)$  are the evaluation of the function  $f$  at the cell nodes. We note that the above quadrature rule uses known information at the vertices of  $\mathcal{T}_h(\Gamma)$ , and thus does not require interpolation as the midpoint would.

*Discrete norms.* We will be using the discrete grid norm  $\|f\|_h$  of a function  $f \in \mathcal{V}_h(\mathcal{T}_h(\Gamma))$  defined as:

$$(13) \quad \|f\|_h^2 = \sum_{T \in \mathcal{T}_h(\Gamma)} \frac{\mathcal{A}_{T_h}}{3} \|f\|_{h,T}^2 = \sum_{T \in \mathcal{T}_h(\Gamma)} \frac{\mathcal{A}_{T_h}}{3} \sum_{j=1}^3 f(\mathbf{p}_j)^2 = \|f_h\|_h^2,$$

where  $f_h = \{f_k\}_1^{N^{dof}} = \{f(\mathbf{p}_k)\}_1^{N^{dof}}$  is the vector of coefficients of the linear combination on the basis of  $\mathcal{V}_h(\mathcal{T}_h(\Gamma))$ . This norm is equivalent to the  $L^2$ -norm and, as a consequence, to the  $H^1$ -norm. In fact, we can write:

$$\|f\|_{L^2(\Gamma)}^2 = \int_{\Gamma} f^2 = \sum_{T \in \mathcal{T}_h(\Gamma)} \int_T \left( \sum_{j=1}^3 f(\mathbf{p}_j) \varphi_j^T \right)^2 = \langle f_h, \mathbf{M} f_h \rangle,$$

The last scalar product can be controlled on both sides by the eigenvalues of the mass matrix  $\mathbf{M}$  to yield:

$$(14) \quad \frac{g^*}{4} \|f_h\|_h^2 \leq \|f\|_{L^2(\Gamma)}^2 \leq g^* \|f_h\|_h^2.$$

*ISFEM formulation.* Now all the ingredients of the ISFEM formulation are completed and we can write:

**Problem 2.3.5** (ISFEM formulation). *Find  $u_h \in \mathcal{V}_h(\mathcal{T}_h(\Gamma))$  such that*

$$a_h(u_h, v_h) = F_h(v_h) \quad \forall v_h \in \mathcal{V}_h(\mathcal{T}_h(\Gamma)),$$

where the linear and bilinear forms are given by:

$$a_h(u_h, v_h) = \sum_{T \in \mathcal{T}_h(\Gamma)} \frac{\mathcal{A}_{T_h}}{3} \sum_{j=1}^3 \langle \mathbb{D}(\mathbf{p}_j) \nabla_{\mathcal{G}} u_h(\mathbf{p}_j), \nabla_{\mathcal{G}} v_h(\mathbf{p}_j) \rangle_{\mathcal{G}},$$

and

$$F_h(v_h) = \sum_{T \in \mathcal{T}_h(\Gamma)} \frac{\mathcal{A}_{T_h}}{3} \sum_{j=1}^3 f_h(\mathbf{p}_j) v_h(\mathbf{p}_j).$$

## 3. NUMERICAL ANALYSIS OF ISFEM

In this section we provide convergence estimates showing that the ISFEM achieves optimal (second order) convergence. Our theoretical results build upon the definition of the basis function  $\varphi_j$  (eq. (11)) and the density estimate in lemma 2.3.2. The standard FEM theory is then adapted to the intrinsic setting. Special attention will be devoted to the analysis of the influence on convergence errors of surface geometric characteristics, such as, e.g., metric tensor and curvatures. For this purpose we will introduce in our analysis different constants. The symbol  $C$  will denote a generic constant not depending on  $h_T$  nor on surface properties. The symbol  $K_i$  will be used to identify constants that are independent of  $h_T$  but depend upon different surface geometric quantities. When working on single elements, we will use the symbol  $K_{i,T}$  to denote the  $i$ -th constant defined on  $T$ .

As usual in FEM theory, this effort will be divided in two parts. First, the local analysis in section 3.1 will develop approximation and interpolation errors on a single triangle. Then, these local results will be combined in section 3.2 to yield the final estimates on the full surface.

**3.1. Approximation errors on triangles.** The strategy used for the proof of lemma 2.3.2 can be employed also in this section. Hence, surface quantities will be written with respect to the local chart  $U_h$  and the inequalities developed on this flat domain. These results can be transferred to the surface element  $T$ , and this will be done in the global estimates of section 3.2. In the following, first, we will summarize some known results involving approximation errors of needed surface quantities using [11, 21] as main references. Then our interpolation and quadrature error estimates will be developed.

**3.1.1. Surface approximation errors.** Given a point  $\mathbf{q} \in T_h$ , we denote by  $\text{pr}(\mathbf{q}) \in T$  the orthogonal projection of  $\mathbf{q}$  onto  $T$  along the direction  $\mathbf{N}(\text{pr}(\mathbf{q}))$ , normal to the surface in  $\text{pr}(\mathbf{q})$ . We state here some results related to the approximation of surface triangles, which can be easily extended to the entire surface. The proofs can be found in [11, lemma 4.1].

**Lemma 3.1.1.** *Given  $T_h$ ,  $T$  and the projection map  $\text{pr}$ , the following estimates hold:*

- *the distance between the approximate triangulation and the surface satisfies:*

$$\max_{\mathbf{q} \in T_h} \left| \overrightarrow{\text{pr}(\mathbf{q})\mathbf{q}} \right| \leq Ch_T^2;$$

- *the ratio  $\delta_h$  between the area measures  $ds$  and  $dx$  of the surface triangle  $T$  and its approximation  $T_h$ , defined by  $ds = \delta_h dx$ , satisfies:*

$$\|1 - \delta_h\|_{L^\infty} \leq Ch_T^2.$$

For any point  $\mathbf{q} \in T_h$ , we define the relative curvature of  $T_h$  with respect to  $\Gamma$  in  $\mathbf{q}$  as follows.

**Definition 3.1.2.** *Given  $W \subset T_h$ , the relative curvature  $\omega_\Gamma(\mathbf{q})$  of any point  $\mathbf{q} \in W$  with respect to  $\Gamma$  is*

$$\omega_\Gamma(\mathbf{q}) = \left| \overrightarrow{\text{pr}(\mathbf{q})\mathbf{q}} \right| \left| \Pi_{\text{pr}(\mathbf{q})} \right|.$$

*Then, the relative curvature of  $W$  is  $\omega_\Gamma(W) = \sup_{\mathbf{q} \in W} \omega_\Gamma(\mathbf{q})$ .*

With reference to [21], we can state the following surface approximation results.

**Lemma 3.1.3.** *Given a geodesic triangulation  $\mathcal{T}_h(\Gamma)$  with surface triangles  $T$  and geodesic edges  $\sigma$ , and their approximations  $T_h$  and  $\sigma_h$  in  $\mathcal{T}_h(\Gamma_h)$ , the following results hold.*

- (1) *The curvilinear length  $\ell_\sigma$  of edge  $\sigma$  is related to the Euclidean length  $\ell_{\sigma_h}$  of the chord  $\sigma_h$  via the inequalities:*

$$\ell_{\sigma_h} \leq \ell_\sigma \leq \frac{1}{1 - \omega_\Gamma(\sigma_h)} \ell_{\sigma_h},$$

where  $\omega_\Gamma(\sigma_h)$  is the relative curvature of  $\sigma_h$  with respect to  $\Gamma$ .

- (2) The difference between the unit vector  $\mathbf{v}_{\overline{\mathbf{p}\mathbf{q}}}$  aligned to the chord  $\sigma_h$  and the unit tangent vector  $\mathbf{t}_{\mathbf{p}}$  to the geodesic edge at  $\mathbf{p}$  satisfies:

$$\left| \mathbf{v}_{\overline{\mathbf{p}\mathbf{q}}} - \mathbf{t}_{\mathbf{p}} \right| \leq \frac{1}{2} |\mathbb{I}_T| \ell_\sigma .$$

- (3) The surface area of the cell  $T$  is related to the planar area of  $T_h$  by the relation:

$$|\mathcal{A}_T - \mathcal{A}_{T_h}| \leq C_T (\theta_{\max}^2 + \omega_\Gamma(T_h)) ,$$

where  $C_T$  is a constant depending on  $T$  and  $\theta_{\max}$  is the maximum over all points  $\mathbf{q} \in T_h$  of the angle between the tangent planes  $T_{\mathbf{q}}T_h$  and  $T_{\text{pr}(\mathbf{q})}T$ .

The following lemma is a straight-forward consequence of the above results:

**Lemma 3.1.4.** For any  $T_h \in \mathcal{T}_h(\Gamma_h)$  we have:

- the relative curvature can be bounded by:

$$\omega_\Gamma(T_h) = \sup_{\mathbf{q} \in T_h} \left| \overrightarrow{\text{pr}(\mathbf{q})\mathbf{q}} \right| |\mathbb{I}_{\text{pr}(\mathbf{q})}| \leq C |\mathbb{I}_T| h_T^2 ;$$

- the maximum angle between tangent planes of  $T$  and  $T_h$  can be bounded by:

$$\theta_{\max} \leq C |\mathbb{I}_T| h_T .$$

3.1.2. *Interpolation and quadrature errors.* We start with estimates of the interpolation errors in  $\mathcal{V}_h(\mathcal{T}_h(\Gamma))$ . We first note that that, using the metric bounds in eq. (3), it is easy to prove the following inequalities relating  $L^2$ -norms of a function  $f$  and its gradient  $\nabla f$  in the cell  $T$  and in the chart  $U_h$  in  $\mathbb{R}^2$ :

$$\begin{aligned} g_{*,T} \|f\|_{L^2(U_h)}^2 &\leq \|f\|_{L^2(T)}^2 = \int_T f^2 = \int_{U_h} f^2 \sqrt{\det(\mathcal{G})} \, ds \leq g_T^* \|f\|_{L^2(U_h)}^2 \\ g_{*,T} c_{*,T} \|\nabla f\|_{L^2(U_h)}^2 &\leq \|\nabla_{\mathcal{G}} f\|_{L^2(T)}^2 = \int_T |\nabla_{\mathcal{G}} f|^2 \\ &= \int_{U_h} |\mathcal{G}^{-1} \nabla f|^2 \sqrt{\det(\mathcal{G})} \, ds \leq g_T^* c_T^* \|\nabla f\|_{L^2(U_h)}^2 \end{aligned}$$

The following Lemma provides the interpolation error estimate for  $I_h(f)$  defined in eq. (11).

**Lemma 3.1.5** (Interpolation error). Given a function  $f \in H^1(T)$ , let  $I_h(f)$  be the ISFEM interpolant in eq. (11). Then, we have:

$$\|f - I_h(f)\|_{L^2(T)} \leq CK_{1,T} h_T^2 \|\partial^2 f\|_{L^2(U_h)} ,$$

$$\|\nabla_{\mathcal{G}} f - \nabla_{\mathcal{G}} I_h(f)\|_{L^2(T)} \leq CK_{2,T} h_T \|\partial^2 f\|_{L^2(U_h)} ,$$

where  $K_{1,T} = \sqrt{g_T^* (1 + C_\phi |\mathbb{I}_T|^2)}$  and  $K_{2,T} = \sqrt{c_T^*} K_{1,T}$ .

*Proof.* Since  $\mathcal{T}_h(\Gamma_h)$  is assumed to be shape-regular, using the standard planar interpolation error and the basis function estimate in lemma 2.3.2, we can write:

$$\begin{aligned} \|f - I_h(f)\|_{L^2(T)}^2 &\leq g_T^* \left( \|f - \pi_1(f)\|_{L^2(U_h)}^2 + \|\pi_1(f) - I_h(f)\|_{L^2(U_h)}^2 \right) \\ &\leq C^2 g_T^* h_T^4 \|\partial^2 f\|_{L^2(U_h)}^2 \left( 1 + C_\phi |\mathbb{I}_T|^2 \right) , \end{aligned}$$

where  $\pi_1(f)$  is the standard  $\mathcal{P}_1$  interpolation polynomial in  $U_h \subset \mathbb{R}^2$ . For the gradient we obtain:

$$\begin{aligned} \|\nabla_{\mathcal{G}} f - \nabla_{\mathcal{G}} I_h(f)\|_{L^2(T)}^2 &\leq c_T^* g_T^* \left[ \|\nabla(f - \pi_1(f))\|_{L^2(U_h)}^2 + \|\nabla(\pi_1(f) - I_h(f))\|_{L^2(U_h)}^2 \right] \\ &\leq C^2 c_T^* g_T^* h_T^2 \|\partial^2 f\|_{L^2(U_h)}^2 \left(1 + C_\phi |\mathbb{I}_T|^2\right). \end{aligned}$$

□

Next, we switch our attention to the accuracy of the surface quadrature rule. Following the results in [3] we show that the surface trapezoidal rule converges with optimal quadratic rate.

**Lemma 3.1.6** (Surface Trapezoidal rule). *Given a function  $f : T \rightarrow \mathbb{R}$ , the surface trapezoidal rule is given by:*

$$Q_{h,T}(f) = \frac{\mathcal{A}_{T_h}}{3} \sum_{j=1}^3 f(\mathbf{p}_j)$$

and satisfies:

$$\left| \int_T f - Q_{h,T}(f) \right| \leq Ch_T^2 \left( \|\partial^2 f\|_{L^2(U_h)} K_{1,T} + \|f\|_{h,T} K_{3,T} \right),$$

where  $f(\mathbf{p}_i)$  is the value of  $f$  at the triangle vertices and  $K_{3,T} = C_T |\mathbb{I}_T| (|\mathbb{I}_T| + 1)$ .

*Proof.* We denote by  $Q(f)$  the surface integral of the projection of  $f$  onto  $\mathcal{V}_h(T)$ , i.e.,  $Q(f) = \int_T I_h(f)$ . Application of the triangular inequality to the quadrature error yields:

$$\left| \int_T f - Q_{h,T}(f) \right| \leq \left| \int_T f - Q(f) \right| + |Q(f) - Q_{h,T}(f)|.$$

From lemma 3.1.5 the first term can be bounded by:

$$\left| \int_T f - Q(f) \right| \leq Ch_T^2 \|\partial^2 f\|_{L^2(U_h)} K_{1,T},$$

while for the second term we use lemma 3.1.3, item 3:

$$\begin{aligned} |Q(f) - Q_{h,T}(f)| &\leq \frac{1}{3} \left| \sum_{j=1}^3 f(\mathbf{p}_j) \right| |\mathcal{A}_T - \mathcal{A}_{T_h}| \leq \frac{1}{3} \left( \sum_{j=1}^3 f(\mathbf{p}_j)^2 \right)^{1/2} |\mathcal{A}_T - \mathcal{A}_{T_h}| \\ &\leq \frac{1}{3} \|f\|_{h,T} C_T (\theta_{\max}^2 + \omega_\Gamma(T_h)) \leq \frac{1}{3} \|f\|_{h,T} C_T |\mathbb{I}_T| (|\mathbb{I}_T| + 1). \end{aligned}$$

Putting the two inequalities together we obtain:

$$\left| \int_T f - Q_{h,T}(f) \right| \leq Ch_T^2 \left( \|\partial^2 f\|_{L^2(U_h)} K_{1,T} + \|f\|_{h,T} C_T |\mathbb{I}_T| (|\mathbb{I}_T| + 1) \right).$$

□

As a remark, we note that, analogously, the midpoint rule is characterized by a similar error estimate, given by:

$$\left| \int_T f - Q_{h,M}(f) \right| \leq Ch_T^2 \left( \|\partial^2 f\|_{L^2(U_h)} K_{1,T} + \|f\|_{\infty,T} K_{3,T} \right),$$

where  $f(\mathbf{m}_T)$  is the value of  $f$  at the centroid  $\mathbf{m}_T$  of  $T$ , having nodal coordinates given by  $\mathbf{s}(\mathbf{m}_T) = \sum_{i=1}^3 \mathbf{s}(\mathbf{p}_i)/3$ .

**3.2. Convergence analysis.** In this section we collect the previously developed local error estimates to build the global estimates forming the overall convergence theory of ISFEM. This analysis proceeds following a standard FEM approach by combining consistency with interpolation errors. Obviously, the developments must take into account the fact that our linear and bilinear ISFEM forms are approximated using the trapezoidal or the midpoint rule. This is handled in a usual fashion with the help of a discrete mesh norm  $\|\cdot\|_h$  which is shown to be equivalent to the  $L^2$ -norm on  $\Gamma$  to show coercivity of the discrete bilinear form. Then the surface extension of Strang Lemma paves the way for the proofs of consistency and then of the final theorems on convergence in  $H^1$  and  $L^2$  norms. The latter, being exactly the surface extension of the Nitsche-Aubin duality trick, is only mentioned without proof. Everything will be done with the implicit assumption that the surface trapezoidal rule is employed. The results for the midpoint rule are exactly the same, and can be proved in a similar way.

We start our task by showing that the discrete bilinear form is coercive.

**Lemma 3.2.1.** *The discrete bilinear form  $a_h(\cdot, \cdot)$  in problem 2.3.5 satisfies:*

$$a_h(v_h, v_h) \geq \frac{d_* \mu_{*, \Gamma}}{g_\Gamma^* (1 + C_\Gamma^2)} \|v_h\|_{H^1(\Gamma)}^2$$

*Proof.* Using the discrete coercivity and Poincaré inequalities, we obtain immediately:

$$\begin{aligned} a_h(v_h, v_h) &= \sum_{T \in \mathcal{T}_h(\Gamma)} \frac{\mathcal{A}_T}{3} \sum_{j=1}^3 \langle \mathbb{D}(\mathbf{p}_j) \nabla_{\mathcal{G}} v_h(\mathbf{p}_j), \nabla_{\mathcal{G}} v_h(\mathbf{p}_j) \rangle_{\mathcal{G}} \\ &\geq d_* \mu_{*, \Gamma} \|\nabla_{\mathcal{G}} v_h\|_h^2 \geq \frac{d_* \mu_{*, \Gamma}}{g_\Gamma^* (1 + C_\Gamma^2)} \|v_h\|_{H^1(\Gamma)}^2. \end{aligned}$$

□

The next step is the surface version of Strang lemma:

**Lemma 3.2.2** (Surface Strang-like Lemma). *Let  $u \in H^1(\Gamma)$  and  $u_h \in \mathcal{V}_h(\mathcal{T}_h(\Gamma))$  be solutions of problem 2.2.1 and problem 2.3.5, respectively. Then, the error  $u - u_h$  satisfies:*

$$\begin{aligned} \|u - u_h\|_{H^1(\Gamma)} &\leq \left( 1 + d^* \frac{g_\Gamma^* (1 + C_\Gamma^2)}{d_* \mu_{*, \Gamma}} \right) \|u - v_h\|_{H^1(\Gamma)} \\ &\quad + \frac{g_\Gamma^* (1 + C_\Gamma^2)}{d_* \mu_{*, \Gamma}} \left( \sup_{w_h} \frac{|a(v_h, w_h) - a_h(v_h, w_h)|}{\|w_h\|_{H^1(\Gamma)}} + \sup_{w_h} \frac{|F(w_h) - F_h(w_h)|}{\|w_h\|_{H^1(\Gamma)}} \right). \end{aligned}$$

*Proof.* From the continuity of  $a(\cdot, \cdot)$  (lemma 2.2.5) and the triangle inequality, we can write for all  $v_h, w_h \in \mathcal{V}_h(\mathcal{T}_h(\Gamma))$ :

$$\begin{aligned} |a_h(u_h - v_h, w_h)| &= |a(u - v_h, w_h) + a(v_h, w_h) - a_h(v_h, w_h) - F(w_h) + F_h(w_h)| \\ &\leq d^* \|u - v_h\|_{H^1(\Gamma)} \|w_h\|_{H^1(\Gamma)} + |a(v_h, w_h) - a_h(v_h, w_h)| + |F(w_h) - F_h(w_h)|. \end{aligned}$$

Using the coercivity of the discrete bilinear form, we obtain:

$$a_h(u_h - v_h, u_h - v_h) \geq \frac{d_* \mu_{*, \Gamma}}{g_\Gamma^* (1 + C_\Gamma^2)} \|u_h - v_h\|_{H^1(\Gamma)} \inf_{w_h} \|w_h\|_{H^1(\Gamma)},$$

or, equivalently:

$$\|u_h - v_h\|_{H^1(\Gamma)} \leq \frac{g_\Gamma^* (1 + C_\Gamma^2)}{d_* \mu_{*, \Gamma}} \sup_{w_h} \frac{|a_h(u_h - v_h, w_h)|}{\|w_h\|_{H^1(\Gamma)}}.$$

Putting together the two inequalities we obtain:

$$\begin{aligned} \|u - u_h\|_{H^1(\Gamma)} &\leq \|u - v_h\|_{H^1(\Gamma)} + \|u_h - v_h\|_{H^1(\Gamma)} \\ &\leq \|u - v_h\|_{H^1(\Gamma)} + \frac{g_\Gamma^*(1 + C_\Gamma^2)}{d_* \mu_{*,\Gamma}} \sup_{w_h} \frac{|a_h(u_h - v_h, w_h)|}{\|w_h\|_{H^1(\Gamma)}}, \end{aligned}$$

from which the result follows.  $\square$

Note that the combination of the estimates of the interpolation error (lemma 3.1.5) and the trapezoidal rule error (lemma 3.1.6) shows that the scheme converges with optimal (first) order of accuracy in the  $H^1(\Gamma)$ -norm. Indeed, it is possible to connect the constants of the error estimates with the geometric characteristics of  $\Gamma$ , as the following consistency lemma states.

**Lemma 3.2.3** (Consistency). *For any continuous and coercive bilinear functional  $a : \mathcal{V}(\Gamma) \times \mathcal{V}(\Gamma) \rightarrow \mathbb{R}$  and any continuous linear functional  $F : \mathcal{V}(\Gamma) \rightarrow \mathbb{R}$  as given in problem 2.2.1, the discrete approximations  $a_h : \mathcal{V}_h(\mathcal{T}_h(\Gamma)) \times \mathcal{V}_h(\mathcal{T}_h(\Gamma)) \rightarrow \mathbb{R}$  and  $F_h : \mathcal{V}_h(\mathcal{T}_h(\Gamma)) \rightarrow \mathbb{R}$  given in problem 2.3.5 are consistent. In other words, we have that for, any  $w_h \in \mathcal{V}_h(\mathcal{T}_h(\Gamma))$ ,*

a) *for the bilinear form  $a(\cdot, \cdot)$ :*

$$(15) \quad |a(v_h, w_h) - a_h(v_h, w_h)| \leq Ch \left( \sqrt{\frac{4K_3 d^*}{g_{*,\Gamma}}} + hK_1 \sqrt{|\Gamma|} \|\mathbb{D}\mathcal{G}^{-1}\|_{H^2(\Gamma)} \right) \|v_h\|_{H^1(\Gamma)} \|w_h\|_{H^1(\Gamma)},$$

where the “broken”  $H^2$ -seminorm  $\|\mathbb{D}\mathcal{G}^{-1}\|_{H^2(\Gamma)}$  is given by:

$$\begin{aligned} \|\mathbb{D}\mathcal{G}^{-1}\|_{H^2(\Gamma)}^2 &= \sum_{T \in \mathcal{T}_h(\Gamma)} \left( \|\partial^2 \mathbb{D}\|_{L^2(T)}^2 + \|\mathbb{D}\|_{L^2(T)}^2 \|\partial^2 \mathcal{G}^{-1}\|_{L^2(T)}^2 \|\mathcal{G}\|_{L^2(T)}^2 \right. \\ &\quad \left. + 4 \|\partial \mathbb{D}\|_{L^2(T)}^2 \|\partial \mathcal{G}^{-1}\|_{L^2(T)}^2 \|\mathcal{G}\|_{L^2(T)}^2 \right); \end{aligned}$$

b) *for the linear form  $F_h(\cdot)$ :*

$$(16) \quad |F(w_h) - F_h(w_h)| \leq Ch \left( \sqrt{\frac{4K_3}{g_{*,\Gamma}}} \|f\|_h + hK_1 \sqrt{|\Gamma|} |f|_{H^2(\Gamma)} \right) \|w_h\|_{H^1(\Gamma)},$$

where the seminorm  $|f|_{H^2(\Gamma)}$  is defined by:

$$|f|_{H^2(\Gamma)}^2 = \|\partial f\|_{L^2(\Gamma)}^2 + \|\partial^2 f\|_{L^2(\Gamma)}^2.$$

*Proof.* The proof is an application of lemmas 3.1.3 and 3.1.5. The general strategy is to use the triangular inequality to separate the interpolation and quadrature terms. Then, the relative error estimates can be used to reach the conclusion.

Starting with the proof of eq. (15), we can write:

$$(17) \quad |a(v_h, w_h) - a_h(v_h, w_h)| \leq \left| \int_\Gamma \langle \mathbb{D} \nabla_\mathcal{G} v_h, \nabla_\mathcal{G} w_h \rangle_\mathcal{G} - \int_\Gamma I_h(\langle \mathbb{D} \nabla_\mathcal{G} v_h, \nabla_\mathcal{G} w_h \rangle_\mathcal{G}) \right| \\ + \left| \int_\Gamma I_h(\langle \mathbb{D} \nabla_\mathcal{G} v_h, \nabla_\mathcal{G} w_h \rangle_\mathcal{G}) - \sum_{T \in \mathcal{T}_h(\Gamma)} \frac{\mathcal{A}_T}{3} \sum_{j=1}^3 \langle \mathbb{D}(\mathbf{p}_j) \nabla_\mathcal{G} v_h(\mathbf{p}_j), \nabla_\mathcal{G} w_h(\mathbf{p}_j) \rangle_\mathcal{G} \right|$$

For better clarity, we denote with  $g = \langle \mathbb{D} \nabla_\mathcal{G} v_h, \nabla_\mathcal{G} w_h \rangle_\mathcal{G}$  the function defined on the surface and with  $\bar{g} = g \circ \phi = \mathbb{D} \mathcal{G}^{-1} \nabla \bar{v}_h \cdot \nabla \bar{w}_h$  when working on the charts  $U$  or  $U_h$ . Then we can write the

first term in the previous equation as:

$$\begin{aligned} \left| \int_{\Gamma} g - \int_{\Gamma} I_h(g) \right| &\leq \sum_{T \in \mathcal{T}_h(\Gamma)} \int_T |g - I_h(g)| \leq C \sum_{T \in \mathcal{T}_h(\Gamma)} \sqrt{\mathcal{A}_T} K_{1,T} h_T^2 \|\partial^2 \bar{g}\|_{L^2(U_h)} \\ &\leq C \sqrt{|\Gamma|} K_1 h^2 \left( \sum_{T \in \mathcal{T}_h(\Gamma)} \|\partial^2 \bar{g}\|_{L^2(U_h)}^2 \right)^{1/2}. \end{aligned}$$

Using the definition of  $g$ , we can estimate the norm of its second derivative as follows:

$$\begin{aligned} \sum_{T \in \mathcal{T}_h(\Gamma)} \|\partial^2 \bar{g}\|_{L^2(U_h)}^2 &\leq \sum_{T \in \mathcal{T}_h(\Gamma)} \left( \|\partial^2 \mathbb{D}\|_{L^2(T)}^2 + 4 \|\partial \mathbb{D}\|_{L^2(T)}^2 \|\partial \mathcal{G}^{-1}\|_{L^2(T)}^2 \|\mathcal{G}\|_{L^2(T)}^2 \right. \\ &\quad \left. + \|\mathbb{D}\|_{L^2(T)}^2 \|\partial^2 \mathcal{G}^{-1}\|_{L^2(T)}^2 \|\mathcal{G}\|_{L^2(T)}^2 \right) \|\nabla v_h\|_{L^2(T)}^2 \|\nabla w_h\|_{L^2(T)}^2 \\ &\leq \|\mathbb{D} \mathcal{G}^{-1}\|_{H^2(\Gamma)}^2 \|v_h\|_{H^1(\Gamma)}^2 \|w_h\|_{H^1(\Gamma)}^2, \end{aligned}$$

where we have used the facts that  $\partial^2 \bar{v}_h = 0$  for any  $v_h \in \mathcal{V}_h(\mathcal{T}_h(U))$  and  $\mathcal{G}^{-1} \nabla \bar{v}_h \cdot \nabla \bar{w}_h = \langle \nabla_{\mathcal{G}} v_h, \nabla_{\mathcal{G}} w_h \rangle_{\mathcal{G}}$ , and we define the ‘‘broken’’  $H^2$ -seminorm  $\|\mathbb{D} \mathcal{G}^{-1}\|_{H^2(\Gamma)}$  element-by-element to allow for flexibility in handling space variable diffusion tensors.

The bound on the second term of eq. (17) rests on the difference between the measures of  $T$  and  $T_h$  via the estimate in lemma 3.1.3. Indeed:

$$\begin{aligned} \left| \int_{\Gamma} I_h(g) - \sum_{T \in \mathcal{T}_h(\Gamma)} \frac{\mathcal{A}_{T_h}}{3} \sum_{j=1}^3 g(\mathbf{p}_j) \right|^2 \\ \leq \sum_{T \in \mathcal{T}_h(\Gamma)} \frac{\mathcal{A}_{T_h}}{9} \sum_{j=1}^3 g(\mathbf{p}_j)^2 \frac{\left| 3 \int_{U_h} \varphi_j \circ \phi \sqrt{\det(\mathcal{G})} \, ds - \mathcal{A}_{T_h} \right|^2}{\mathcal{A}_{T_h}}. \end{aligned}$$

Using the definition of discrete grid norm in eq. (13) and the fact that  $\varphi_j \circ \phi \leq 1$ , the above inequality can be developed further as:

$$\begin{aligned} \sum_{T \in \mathcal{T}_h(\Gamma)} \frac{\mathcal{A}_{T_h}}{9} \sum_{j=1}^3 g(\mathbf{p}_j)^2 \frac{\left| 3 \int_{U_h} \varphi_j \circ \phi \sqrt{\det(\mathcal{G})} \, ds - \mathcal{A}_{T_h} \right|^2}{\mathcal{A}_{T_h}} \\ \leq \frac{1}{3} \|g\|_h^2 \sup_{T \in \mathcal{T}_h(\Gamma)} 9 \frac{|\mathcal{A}_T - \mathcal{A}_{T_h}|^2}{\mathcal{A}_{T_h}} \leq 3K_3 h^2 \|g\|_h^2, \end{aligned}$$

where  $K_3 = \max_T K_{3,T}$ , with  $K_{3,T}$  defined in lemma 3.1.6 (see also lemma 3.1.3, item 3). Recalling that  $\|g\|_h = \|I_h(g)\|_h$  and  $g = \langle \mathbb{D} \nabla_{\mathcal{G}} v_h, \nabla_{\mathcal{G}} w_h \rangle_{\mathcal{G}}$ , we obtain:

$$\left| \int_{\Gamma} I_h(g) - \sum_{T \in \mathcal{T}_h(\Gamma)} \frac{\mathcal{A}_{T_h}}{3} \sum_{j=1}^3 g(\mathbf{p}_j) \right|^2 \leq 3K_3 h^2 \frac{4}{g_{*,\Gamma}} d^* \|v_h\|_{H^1(\Gamma)}^2 \|w_h\|_{H^1(\Gamma)}^2.$$

The final consistency estimate for the quadrature-based bilinear form then becomes:

$$\begin{aligned} |a(v_h, w_h) - a_h(v_h, w_h)| \\ \leq Ch \left( \sqrt{\frac{4K_3 d^*}{g_{*,\Gamma}}} + hK_1 \sqrt{|\Gamma|} \|\mathbb{D} \mathcal{G}^{-1}\|_{H^2(\Gamma)} \right) \|v_h\|_{H^1(\Gamma)} \|w_h\|_{H^1(\Gamma)}. \end{aligned}$$

The proof of eq. (16) proceeds analogously with  $g$  replaced by  $fw_h$ .

□

The previous lemma together with the interpolation and quadrature errors yield the main convergence theorem for ISFEM.

**Theorem 3.2.4** (Optimal  $H^1$ -norm convergence). *The ISFEM approach converges in the  $H^1$ -norm with optimal first order accuracy:*

$$\|u - u_h\|_{H^1(\Gamma)} \leq \mathbb{C}_1 h \|f\|_{L^2(\Gamma)} + \mathbb{C}_2 h^2 \|f\|_{H^2(\Gamma)}$$

where the constants  $\mathbb{C}_1, \mathbb{C}_2$  depend on the surface  $\Gamma$  and its geometrical characteristics, and on the upper and lower bounds of the diffusion tensor  $\mathbb{D}$ .

*Proof.* The proof is a direct application of the previous two lemmas. Indeed, including the consistency estimates into the surface Strang-like lemma we obtain:

$$\begin{aligned} \|u - u_h\|_{H^1(\Gamma)} &\leq \left(1 + d^* \frac{g_\Gamma^*(1 + C_\Gamma^2)}{d_* \mu_{*,\Gamma}}\right) \|u - v_h\|_{H^1(\Gamma)} \\ &\quad + \frac{g_\Gamma^*(1 + C_\Gamma^2)}{d_* \mu_{*,\Gamma}} \left( \sup_{w_h} \frac{|a(v_h, w_h) - a_h(v_h, w_h)|}{\|w_h\|_{H^1(\Gamma)}} + \sup_{w_h} \frac{|F(w_h) - F_h(w_h)|}{\|w_h\|_{H^1(\Gamma)}} \right) \\ &\leq C \left(1 + d^* \frac{g_\Gamma^*(1 + C_\Gamma^2)}{d_* \mu_{*,\Gamma}}\right) \frac{(K_2 + K_1 h)}{g_{*,\Gamma}} h \|\partial^2 u\|_{L^2(\Gamma)} \\ &\quad + C \frac{g_\Gamma^*(1 + C_\Gamma^2)}{d_* \mu_{*,\Gamma}} \left[ \left(\frac{4K_3}{g_{*,\Gamma}}\right)^{\frac{1}{2}} \left(\sqrt{d^*} \|I_h(u)\|_{H^1(\Gamma)} + \|f\|_h\right) \right. \\ &\quad \left. + h K_1 |\Gamma|^{\frac{1}{2}} \left(\|\mathbb{D} \mathcal{G}^{-1}\|_{H^2(\Gamma)} \|I_h(u)\|_{H^1(\Gamma)} + |f|_{H^2(\Gamma)}\right) \right] h, \end{aligned}$$

where we chose  $v_h = I_h(u)$  and we used the inequality:

$$\begin{aligned} \|v_h\|_{H^1(\Gamma)}^2 &\leq \frac{g_\Gamma^*(1 + C_\Gamma^2)}{d_* \mu_{*,\Gamma}} a_h(v_h, v_h) \\ &= \frac{g_\Gamma^*(1 + C_\Gamma^2)}{d_* \mu_{*,\Gamma}} F_h(v_h) \leq \frac{g_\Gamma^*(1 + C_\Gamma^2)}{d_* \mu_{*,\Gamma}} \sqrt{\frac{4|\Gamma|}{3g_{*,\Gamma}}} \|f_h\|_{L^2(\Gamma)} \|v_h\|_{L^2(\Gamma)} \end{aligned}$$

□

The estimate in the above theorem contains on the right-hand-side a standard term related to the interpolation error plus a second term that goes to zero for a flat surface and it is thus compatible with standard FEM  $\mathcal{P}_1$  estimates. Finally, we conclude this section by mentioning only that using the standard duality arguments optimal  $L^2$  convergence is obtained.

#### 4. NUMERICAL EXPERIMENTS

In this section we provide numerical support to the results presented in the previous sections. We present two different numerical experiments. In the first test case the aim is to show that the value of the constant in the  $L^2$ -error for the solution and its gradient increases while the maximum value of the curvature increases. The second test case shows that the ISFEM method can be directly applied in the presence of multiple charts, if compatible sets of tangent vectors are available. Both test cases were considered already in [5] for the case of advection-diffusion-reaction equation discretized on the chart and numerically solved by means of a geometrically intrinsic version of the virtual element method. For the test case 2, we extend the result in [5] by directly



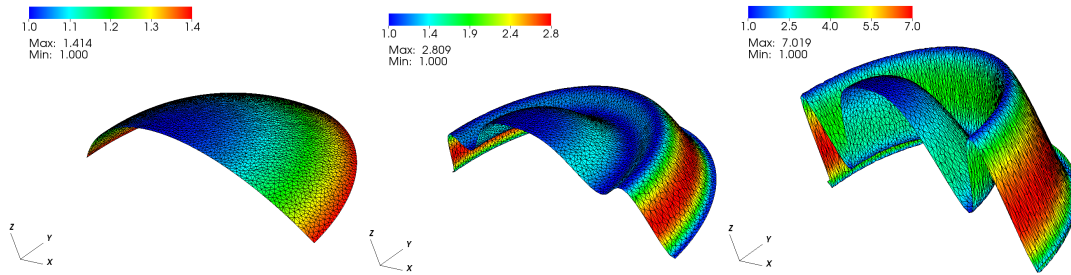


FIGURE 1. Surfaces described by eq. (18) with  $r = 2$ ,  $k = 5$  and  $a = 0, 0.5, 2$ , respectively in the left, middle and right panels. The color map shows the value of  $\sqrt{\det(\mathcal{G}(\Gamma))}$ .

solving the equation on the sphere, without the use of extra conditions at the interface of the two charts.

In all the experiments we consider a manufactured solution  $u : \Gamma \rightarrow \mathbb{R}$  and calculate the resulting forcing function  $f$  by substitution into the original equation. Note that, even a simple manufactured solution would become highly nonlinear when considered on a surface, due to the spatially varying geometric information.

**Test case 1.** For the test case 1 we consider the surface provided by the graph of the following height function (see [5]):

$$(18) \quad x^3 = \mathcal{H}(x^1, x^2) = \sqrt{r - (x^1)^2 - (x^2)^2 + a \cos^2\left(k \frac{\pi}{2} ((x^1)^2 + (x^2)^2)\right)},$$

a trigonometric perturbation of a sphere, where  $r$  is the radius of the sphere, and  $a$  and  $k$  are the amplitude and the frequency of the cosine trigonometric perturbation. We use the parametrization  $\Gamma = \{(x^1, x^2, \mathcal{H}(x^1, x^2)) \mid x^2 \geq 0 \text{ and } (x^1)^2 + (x^2)^2 \geq 1\}$ , a radius  $r = 2$  and a frequency  $k = 5$ . Figure 1 shows the surfaces obtained with different values of the amplitude  $a$ : a sphere ( $a = 0$ ) is shown in the left panel, and two trigonometric deformations of the sphere are shown in the middle and left panels for the case  $a = 0.5$  and  $a = 2$ , respectively. The color map shows the distribution in space of  $\sqrt{\det(\mathcal{G}(\Gamma))}$ . The mesh sets used in this test case are obtained from subsequent refinements of Delaunay triangulations of  $U = \{(x^1, x^2) \mid x^2 \geq 0 \text{ and } (x^1)^2 + (x^2)^2 \geq 1\}$ , then elevated using the height function eq. (18). We consider 8 levels of refinement, with a initial value of the surface mesh parameter  $h \approx 0.25$  at  $\ell = 0$ . This corresponds to a total of 70 surface nodes for the case of  $a = 0$  and  $a = 0.05$ , while for the case  $a = 2$  the total number of nodes is 265 for  $\ell = 0$ . We define  $u = x^1$  as manufactured solution and we compute an expression for the forcing function by the equation  $f(s^1, s^2) = -\Delta_{\mathcal{G}} u$ . We apply Dirichlet boundary condition by imposing the exact solution at the boundary nodes.

Figure 2 shows the  $L^2$ -errors and experimental orders of convergence for the solution and its gradient. We notice second order convergence rates for the solution and first order for the gradient. Convergence rates slightly different than the optimal ones at the initial levels are attributable to a too coarse resolution of the surface triangulation, not accurate enough to approximate the surface. In particular, this phenomenon can be observed in the case of higher values of the parameter  $a$  that corresponds to higher values of the surface curvature.

**Test case 2.** We consider here  $\Gamma = S^2$ . We use two parametrizations, one for the northern and one for the southern hemispheres, to define two sets of tangent vectors and consider the equator as intersection set. A smooth transition map is known in this particular case. The stereographic

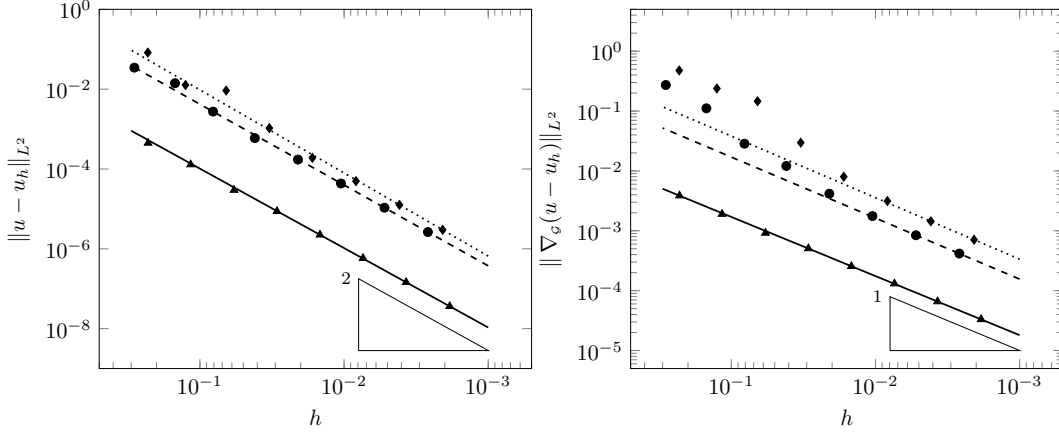


FIGURE 2. TC1: Numerical convergence of  $L^2$ -errors for the solution (left) and its gradient (right) vs  $h$  on the surface triangulation. The convergence lines are obtained by means of least-square approximation considering the last 2 point values. The different lines denote the three different values of  $a$  considered: solid line with triangular data points is used for the case  $a = 0$ , dashed line with circular data points for  $a = 0.5$ , and dotted line with diamond data points for the case  $a = 2$ . The optimal theoretical slope is represented by the lower right triangles.

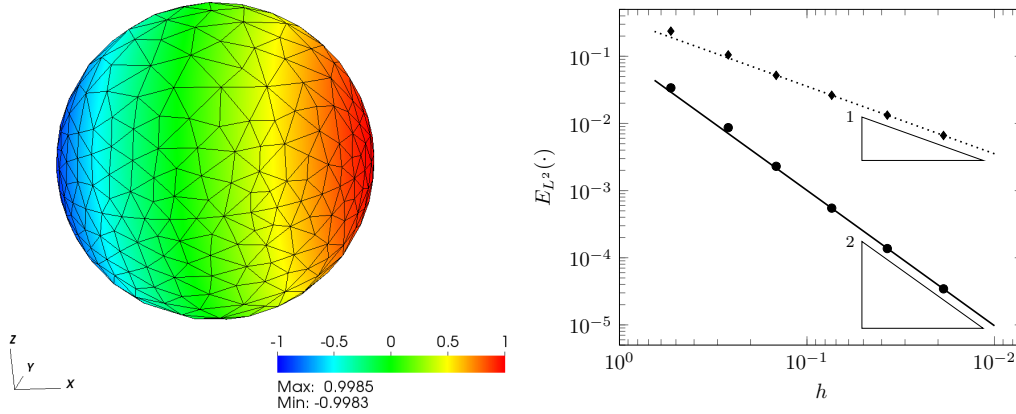


FIGURE 3. TC2: Numerical solution on the sphere (mesh level  $\ell = 1$ ), left panel, and numerical convergences in the  $L^2$ -norm for both the solution (solid line with circular data points) and its gradient (dotted line with diamond data points), right panel. The convergence lines are obtained by approximating via least-square the last 3 point values.

projections for the northern hemisphere is given by:

$$(19) \quad \phi_N(s^1, s^2) = \left( \frac{2s^1}{1 + (s^1)^2 + (s^2)^2}, \frac{2s^2}{1 + (s^1)^2 + (s^2)^2}, \frac{1 - (s^1)^2 - (s^2)^2}{1 + (s^1)^2 + (s^2)^2} \right) = (x^1, x^2, x^3),$$

and similarly for the southern hemisphere, with the transition map between north and south written as:

$$\psi(s_N^1, s_N^2) = \left( \frac{s_N^1}{(s_N^1)^2 + (s_N^2)^2}, \frac{s_N^2}{(s_N^1)^2 + (s_N^2)^2} \right) = (s_s^1, s_s^2).$$

The surface triangulation of the sphere is obtained by computing a Delaunay triangulation of the disk,  $U = \{(x^1, x^2) \mid (x^1)^2 + (x^2)^2 \leq 1\}$ , then projecting the points to the surface using the two stereographic projections. We consider a set of meshes with 6 levels of refinement, with a initial value of the surface mesh parameter  $h = 0.532$  and a total of 111 surface nodes. Analogously to the first test case, we assume  $u = x^1$  and compute the forcing function by  $f(s^1, s^2) = -\Delta_g u + u$ . Note that in the case of the stereographic projection  $x^1 \neq s^1$ . We need to make use of the inverse of eq. (19) (as well as the south projection) to compute the forcing function in the variables  $s^1, s^2$ . Figure 3 show on the left the manufactured solution and on the right the  $L^2$ -errors and experimental orders of convergence for the solution and its gradient. Again, we notice an optimal order of convergence rates for both the solution and the gradient.

#### ACKNOWLEDGMENTS

The first author wishes to thank the German Research Foundation (DFG) for financial support within the Research Unit ‘‘Vector- and Tensor-Valued Surface PDEs’’ (FOR 3013) with project no. VO 899/22-1.

#### REFERENCES

- [1] M. Abate and F. Tovena. *Curves and Surfaces*. Springer-Verlag Italia, Milano, Italy, 2012.
- [2] P. F. Antonietti, A. Dedner, P. Madhavan, S. Stangalino, B. Stinner, and M. Verani. High order discontinuous Galerkin methods for elliptic problems on surfaces. *SIAM J. Num. Anal.*, 53(2):1145–1171, Jan. 2015.
- [3] E. Bachini and M. Putti. Geometrically intrinsic modeling of shallow water flows. *ESAIM Math. Model. Num. Anal.*, 54(6):2125–2157, 2020. doi: 10.1051/m2an/2020031.
- [4] E. Bachini, M. W. Farthing, and M. Putti. Intrinsic finite element method for advection-diffusion-reaction equations on surfaces. *J. Comp. Phys.*, 424, 2021. doi: 10.1016/j.jcp.2020.109827.
- [5] E. Bachini, G. Manzini, and M. Putti. Arbitrary-order intrinsic virtual element method for elliptic equations on surfaces. *Calcolo*, 58(30), 2021.
- [6] M. Bertalmio, L.-T. Cheng, S. Osher, and G. Sapiro. Variational problems and partial differential equations on implicit surfaces. *J. Comp. Phys.*, 174(2):759–780, Dec. 2001.
- [7] F. Bouchut and M. Westdickenberg. Gravity driven shallow water models for arbitrary topography. *Comm. Math. Sci.*, 2(3):359–389, Sept. 2004.
- [8] E. Burman, P. Hansbo, M. G. Larson, K. Larsson, and A. Massing. Finite element approximation of the Laplace–Beltrami operator on a surface with boundary. *Numer. Math.*, 141(1): 141–172, July 2018.
- [9] P. G. Ciarlet. *Linear and Nonlinear Functional Analysis with Applications*. SIAM, Oct. 2013.
- [10] G. Dziuk. Finite-elements for the Beltrami operator on arbitrary surfaces. *Lecture Notes in Mathematics*, 1357:142–155, 1988.
- [11] G. Dziuk and C. M. Elliott. Finite element methods for surfaces PDEs. *Acta Num.*, 22: 289–396, 2013.
- [12] I. Fent, M. Putti, C. Gregoretto, and S. Lanzoni. Modeling shallow water flows on general terrains. *Adv. Water Resour.*, 121:316–332, 2018.
- [13] E. D. Fernández-Nieto, F. Bouchut, D. Bresch, M. J. Castro Díaz, and A. Mangeney-Castelnau. A new Savage–Hutter type model for submarine avalanches and generated tsunami. *J. Comp. Phys.*, 227(16):7720–7754, Aug. 2008.

- [14] A. Ferroni, L. Formaggia, and A. Fumagalli. Numerical analysis of Darcy problem on surfaces. *ESAIM Math. Model. Num. Anal.*, 50(6):1615–1630, Oct. 2016.
- [15] N. Flyer, E. Lehto, S. Blaise, G. B. Wright, and A. St-Cyr. A guide to RBF-generated finite differences for nonlinear transport: Shallow water simulations on a sphere. *J. Comp. Phys.*, 231(11):7133–7151, June 2012.
- [16] M. Frittelli and I. Sgura. Virtual element method for the Laplace-Beltrami equation on surfaces. *ESAIM Math. Model. Num. Anal.*, 52(3):965–993, Sept. 2018.
- [17] K. Georg and J. Tausch. Some error estimates for the numerical approximation of surface integrals. *Math. Comp.*, 62(206):755–763, 1994.
- [18] E. Hebey. *Nonlinear Analysis on Manifolds: Sobolev Spaces and Inequalities: Sobolev Spaces and Inequalities*, volume 5. American Mathematical Soc., 2000.
- [19] P. Li. *Geometric Analysis*. Cambridge Studies in Advanced Mathematics. Cambridge University Press, 2012. doi: 10.1017/CBO9781139105798.
- [20] J. Lowengrub, J. Allard, and S. Aland. Numerical simulation of endocytosis: Viscous flow driven by membranes with non-uniformly distributed curvature-inducing molecules. *J. Comp. Phys.*, 309:112–128, 2016. doi: <https://doi.org/10.1016/j.jcp.2015.12.055>.
- [21] J.-M. Morvan. *Generalized Curvatures*, volume 2 of *Geometry and Computing*. Springer Science & Business Media, Berlin, Heidelberg, May 2008.
- [22] M. P. Neilson, J. A. Mackenzie, S. D. Webb, and R. H. Insall. Modeling cell movement and chemotaxis using pseudopod-based feedback. *SIAM J. Sci. Comput.*, 33(3):1035–1057, Jan. 2011.
- [23] M. Nestler, I. Nitschke, and A. Voigt. A finite element approach for vector- and tensor-valued surface pdes. *J. Comp. Phys.*, 389:48–61, 2019. ISSN 0021-9991. doi: <https://doi.org/10.1016/j.jcp.2019.03.006>. URL <https://www.sciencedirect.com/science/article/pii/S0021999119301895>.
- [24] I. Nitschke, A. Voigt, and J. Wensch. A finite element approach to incompressible two-phase flow on manifolds. *J. Fluid Mech.*, 708:418, 2012.
- [25] O. Sander. Geodesic finite elements for cosserat rods. *Int. J. Numer. Methods Engrg.*, 82(13):1645–1670, 2010. doi: <https://doi.org/10.1002/nme.2814>.
- [26] O. Sander. Geodesic finite elements on simplicial grids. *Int. J. Numer. Methods Engrg.*, 92(12):999–1025, 2012.
- [27] C. Stöcker and A. Voigt. Geodesic evolution laws—A level-set approach. *SIAM J. Imag. Sci.*, 1(4):379–399, 2008. doi: 10.1137/070699640.
- [28] M. E. Taylor. *Partial Differential Equations I: Basic Theory*. Applied Mathematical Sciences. Springer New York, 2010.

INSTITUTE OF SCIENTIFIC COMPUTING, TU DRESDEN, GERMANY  
 Email address: elena.bachini@tu-dresden.de

DEPARTMENT OF MATHEMATICS “TULLIO LEVI-CIVITA” UNIVERSITY OF PADUA, ITALY  
 Email address: mario.putti@unipd.it